

Transition from band insulator to Mott insulator in one dimension: Critical behavior and phase diagram

Jizhong Lou,^{1,2} Shaojin Qin,^{1,3} Tao Xiang,¹ Changfeng Chen,² Guang-Shan Tian,⁴ and Zhaobin Su¹

¹*Institute of Theoretical Physics, P. O. Box 2735, Beijing 100080, China*

²*Department of Physics, University of Nevada, Las Vegas, Nevada 89154*

³*Department of Physics, Kyushu University, Hakozaki, Higashi-ku, Fukuoka 812-8581, Japan*

⁴*Department of Physics, Peking University, Beijing 100087, China*

(Dated: November 17, 2018)

We report a systematic study of the transition from band insulator (BI) to Mott insulator (MI) in a one-dimensional Hubbard model with an on-site Coulomb interaction U and an alternating periodic site potential V . We employ both the zero-temperature density matrix renormalization group (DMRG) method to determine the gap and critical behavior of the system and the finite-temperature transfer matrix renormalization group (TMRG) method to evaluate the thermodynamic properties. We find two critical points at $U = U_c$ and $U = U_s$ that separate the BI and MI phases for a given V . A charge-neutral spin-singlet exciton band develops in the BI phase ($U < U_c$) and drops below the band gap when U exceeds a special point U_c . The exciton gap closes at the first critical point U_c while the charge and spin gaps persist and coincide between $U_c < U < U_s$ where the system is dimerized. Both the charge and spin gaps collapse at $U = U_s$ when the transition to the MI phase occurs. In the MI phase ($U > U_s$) the charge gap increases almost linearly with U while the spin gap remains zero. These findings clarify earlier published results on the same model and offer new insights into several important issues regarding appropriate scaling analysis of DMRG data and a full physical picture for the delicate nature of the phase transitions driven by electron correlation. The present work provides a comprehensive understanding for the critical behavior and phase diagram for the transition from BI to MI in one-dimensional correlated electron systems with a periodic alternating site potential.

PACS numbers: 71.30.+h, 71.10.Pm, 77.80.-e

I. INTRODUCTION

The nature of the insulating ground state of interacting electron systems has been a subject of long-standing interest and debate in condensed matter physics. Because of strong quantum effects caused by spatial confinement and technical advantages for theoretical treatment, one-dimensional (1D) electron systems have been most extensively studied^{1,2}. Strong correlation effects in 1D lead to the separation (decoupling) of charge and spin degrees of freedom. Starting from a gapless phase with charge-spin separated excitations, interactions can drive the system into new phases of different characteristics with (i) gapful charge excitations only, (ii) gapful spin excitations only, or (iii) co-existing gapful charge and spin excitations. For phases with both charge and spin excitations gapful, the charge and spin degrees of freedom are rarely decoupled. Despite these findings, there remain important unresolved issues regarding the quantum nature of the insulating state in 1D interacting electron systems and the phase transitions driven by the electron correlation. The first issue concerns the establishment of an accurate phase diagram and the critical behavior near the phase boundaries. Secondly, a band insulator (BI) with quasi-particle excitations typically cannot be characterized by charge and spin excitations. A proper characterization scheme needs to be developed. Most importantly, the nature of the correlation-driven transition from BI to Mott insulator (MI) is still not fully understood.

There has been considerable recent interest in the study of a prototype one-dimensional model for ferroelectric perovskites for the understanding of the response of strongly correlated electron systems with lattice distortions. These efforts have raised and addressed some fundamental issues in the nature of the quantum phase transition and the related critical behavior in 1D interacting electron systems. Earlier works^{3,4,5} mainly deal with the effects of strong electron correlation on the electron-lattice interaction and the polarization effects in the insulator. Quantum phase transitions and the characterization of the insulating state are the focus of more recent work.^{6,7,8,9,10,11,12,13,14,15,16} In particular, an issue of fascinating debate is the nature of the transition (or crossover) from the BI phase to the MI phases. Gidopoulos *et al.* showed¹⁷ that due to the reversal of inversion symmetry of the ground state from BI to MI, there is a critical point for spin excitations. However, for charge excitations the critical behavior is less clear. Recently, Fabrizio *et al.*¹⁸ developed an effective field theory for this problem and showed that there are two continuous transitions from BI to MI. One is a spin transition of the Kosterlitz-Thouless type at a critical point $U = U_s$, and the other is an exciton transition at an Ising critical point $U = U_c < U_s$ where the exciton gap closes. Between U_c and U_s , the site-parity is spontaneously broken and the system is characterized by a doubly degenerate, dimerized ground state. These results raise interesting questions about the structure of the ground-state phase

diagram of 1D interacting electron systems and the characterization of the critical behavior near the transition points from the BI phase to the MI phase.

The model Hamiltonian for the system of interest is defined in the Hubbard formalism at half-filling^{5,6,7,9,19}

$$H = \sum_{i\sigma} \left[-t \left(c_{i\sigma}^\dagger c_{i+1\sigma} + \text{h.c.} \right) + V(-1)^i n_{i\sigma} \right] + U \sum_i \left(n_{i\uparrow} - \frac{1}{2} \right) \left(n_{i\downarrow} - \frac{1}{2} \right), \quad (1)$$

where $c_{i\sigma}^\dagger$ and $n_{i\sigma}$ are the electron creation and number operators at site i , $U > 0$ is the on-site Coulomb repulsion, and V is the staggered site chemical potential. This model captures the key ingredients of one-dimensional correlated insulators with mixed ionic-covalent characters, such as oxide dielectric materials²⁰ and quasi-1D organic charge-transfer complexes.²¹ It incorporates covalency, ionicity, and strong electron correlation.^{3,4}

In this paper, we present the results of extensive calculations for Hamiltonian (1) using both the zero-temperature density matrix renormalization group (DMRG) method²² and the finite-temperature transfer matrix renormalization group (TMRG) method^{23,24,25}. These methods have been demonstrated to be highly accurate for 1D interacting electron systems. Our aim is to systematically examine and clarify issues raised in recent work and to provide a comprehensive understanding for the transition from BI to MI in one dimension. We show detailed results on the gap and critical behavior. We find that a charge-neutral spin-singlet exciton band forms in the BI phase and drops below the band gap as U increases beyond a special point U_e . With increasing U the excitons then condense and the system enters a dimerized phase, followed by the closure of the quasi-particle (both spin and charge) gap when the system enters the MI phase. We clarify basic concepts on charge and spin excitations studied in recent work. Our results support the conclusion of Fabrizio *et al.*¹⁸ on the existence of two critical points for the transition from BI to MI. We also present detailed results on the formation of the exciton band and the scaling behavior near the critical points. In addition, we carry out TMRG calculations to study thermodynamic properties to further elucidate the gap and critical behavior of the system.

II. LOW-ENERGY EXCITATIONS

To properly characterize the BI and MI phases and establish the phase diagram, we need to evaluate the behavior of several low-energy excitations, including the charge and spin excitations and an exciton excitation that will be used to characterize the BI phase. We calculate the following three excitation gaps defined on a finite 1D lattice of length L (chosen as an even integer) at half-filling: (i) the singlet exciton gap $\Delta_e(L)$, (ii) the charge gap

$\Delta_c(L)$, and (iii) the spin-triplet gap $\Delta_s(L)$,

$$\Delta_e(L) = E_1\left(\frac{L}{2}, \frac{L}{2}\right) - E_0\left(\frac{L}{2}, \frac{L}{2}\right), \quad (2)$$

$$\Delta_c(L) = E_0\left(\frac{L}{2} + 1, \frac{L}{2}\right) + E_0\left(\frac{L}{2} - 1, \frac{L}{2}\right) - 2E_0\left(\frac{L}{2}, \frac{L}{2}\right), \quad (3)$$

$$\Delta_s(L) = E_0\left(\frac{L}{2} + 1, \frac{L}{2} - 1\right) - E_0\left(\frac{L}{2}, \frac{L}{2}\right), \quad (4)$$

where $E_0(N_\uparrow, N_\downarrow)$ is the lowest energy of the system with N_\uparrow up and N_\downarrow down spin electrons, and $E_1(N_\uparrow, N_\downarrow)$ is the lowest energy of the singlet excitations. For the charge gap Δ_c , there is an alternative definition

$$\Delta_c(L) = E\left(\frac{L}{2} + 1, \frac{L}{2} + 1\right) - E\left(\frac{L}{2}, \frac{L}{2}\right). \quad (5)$$

For the model studied in this work, these two definitions on the charge gap give the same results in the thermodynamic limit. This is supported by our numerical calculations. However, since the numerical accuracy is much higher in calculating Δ_c by using Eq. (3) than by using Eq. (5), we use Eq. (3) in all the reported calculations.

Although Δ_c and Δ_s are usually considered to be the charge gap and the spin gap, respectively, in the literature, Δ_c in fact is the chemical potential jump for particles in the system. It measures the chemical potential jump of putting a particle into or taking a particle out of the system. Only when the charge and spin excitations are separated and the spin gap is zero, Δ_c is equal to the charge excitation gap as, for example, in the standard Hubbard model (Eq. (1) with $V = 0$ or $U \rightarrow \infty$). When the charge and spin excitations are not separated, or when the spin gap is not zero, the chemical potential jump is not equal to the charge excitation gap.

At half-filling, the first excitation state can be either a spin singlet or a spin triplet and Δ_e never exceeds Δ_s . When $\Delta_e < \Delta_s$, the first excitation state must be a charge-neutral spin-singlet state; otherwise, Δ_e equals Δ_s and measures the excitation gap of an exciton band.

In the presence of a nonzero V in the Hamiltonian, the MI phase is reached when U is large (including the limit $U \rightarrow \infty$). In the MI phase, it is well understood that the charge gap is non-zero, but the spin gap is zero. Therefore Δ_c is the charge excitation gap. Meanwhile, both Δ_s and Δ_e are zero and the gapless elementary excitations in the system are spinons.²⁶

In the BI phase, all the elementary excitations are gapful. Let $u_{k\sigma}^\dagger$ and $d_{k\sigma}^\dagger$ be the creation operators for particles in the upper conducting band and for the holes in the lower valence band. The Hamiltonian for free particles at $U = 0$ is

$$H = \sum_{k\sigma} \varepsilon_k \left(u_{k\sigma}^\dagger u_{k\sigma} - v_{k\sigma}^\dagger v_{k\sigma} \right), \quad (6)$$

where k is the momentum, σ is the spin index, and $\varepsilon_k = \sqrt{V^2 + 4t^2 \cos^2 k}$. We have $u_{k\sigma} |GS\rangle = v_{k\sigma}^\dagger |GS\rangle = 0$ for the ground state $|GS\rangle$ at half filling with $u_{k\sigma}$ being the annihilation operator for electrons in the conduction band, and $v_{k\sigma}^\dagger$ the creation operator for electrons

in the valence band. For particle-hole excitations with one particle and one hole in the system, it is clear that $\Delta_c = \Delta_s = \Delta_e = 2V$.

When U is small in the BI phase, the particle or hole excitations become dressed quasi-particles, and Δ_c measures the chemical potential jump of the particles. Since the charge and spin degrees of freedom are not separated, Δ_c is not exactly the "charge gap" derived from the gapless charge-spin separated excitations in the field theoretical approach. If the particles and holes are not bounded, then $\Delta_c = \Delta_s = \Delta_e$. However, the particle-hole excitations may bound to form excitons, and result in an exciton gap smaller than Δ_c . It is confirmed by our DMRG calculations shown below that Δ_e equals Δ_c when U is small, but becomes smaller than Δ_c when U exceeds a special point U_e , indicating the formation of singlet excitons. Meanwhile, the calculations show that $\Delta_s = \Delta_c$ is always observed, indicating that there is no triplet exciton formation in the BI phase.

The DMRG calculations also show that in the BI phase the exciton gap and quasi-particle excitation gap decrease and approach zero with increasing U . The exciton gap closes at the first critical point U_c , and the system enters a phase where the excitons condense to form dimerized ground state. At the second critical point U_s the quasi-particle gap also closes ($\Delta_e = \Delta_s = \Delta_c = 0$). When U exceeds U_s , Δ_e and Δ_s remain zero but Δ_c increases almost linearly with U . Therefore, U_s is the point where the quasi-particle excitation gap in the BI phase collapses, and spinons in the MI phase form. This picture is consistent with that of the recent field theoretical studies¹⁸.

From the physical picture outlined above, it is clear that there are three special points U_e , U_c , and U_s along the U scale. Among them U_c and U_s are two critical points separating the BI and MI phases while U_e is a special point signaling the formation of the spin-singlet exciton band in the BI phase. In the thermodynamic limit for a given V the system can be divided into the following regions:

1. $0 < U < U_e$, $\Delta_e = \Delta_c = \Delta_s \neq 0$, gapful quasi-particle excitations only.
2. $U_e < U < U_c$, $0 < \Delta_e < \Delta_c = \Delta_s$, gapful quasi-particle excitations coexist with singlet particle-hole excitations that bound to form excitons.
3. $U = U_c$, $\Delta_e = 0$, $\Delta_c = \Delta_s > 0$, the system is critical for exciton excitations.
4. $U_c < U < U_s$, $\Delta_e < \Delta_c = \Delta_s$, excitons condense, and the system is dimerized.
5. $U = U_s$, $\Delta_e = \Delta_c = \Delta_s = 0$, the system is critical for quasi-particle excitations.
6. $U > U_s$, $\Delta_e = \Delta_s = 0$, $\Delta_c > 0$, gapless spinon excitations in the MI phase; the particle-hole picture breaks down.

In the following we present the calculated results on the gap and critical behavior leading to the establishment of the phase diagram. In all reported calculations, free boundary conditions are used in the zero-temperature DMRG calculation. For a finite size system, we can show rigorously using the variational principle that the lowest energy state of the Hamiltonian (1) with free boundary conditions in each $(N_\uparrow, N_\downarrow)$ subspace is non-degenerate except for an up-down spin degeneracy²⁸. Therefore there is no level crossing with the lowest energy state in the $(N_\uparrow, N_\downarrow)$ subspace and $E_0(N_\uparrow, N_\downarrow)$ is an analytic function of U and V . From this property and Eqs. (3) and (4), we can further show that $\Delta_c(L)$ and $\Delta_s(L)$ are also analytic functions of U and V . In this work we focus on two values of the staggered potential $V=0.3t$ and $1.0t$ and study the behavior of the three gaps introduced above in response to the on-site Coulomb repulsion U .

III. EXCITATION GAPS

For fermion systems, the truncation error of DMRG iterations is generally much smaller than that of spin systems when the same number of optimal states are retained. The efficiency of the finite system DMRG method is related to the truncation error; the bigger the truncation error is, the larger the improvement of the finite lattice sweeping can make. We used both finite and infinite lattice DMRG algorithms in testing calculations. We find that the improvement of the ground-state energy made with the finite lattice sweeping is very small when a large number of states are retained. A better way to increase the accuracy of the results is using the infinity lattice approach by retaining more states.

Figure 1 shows the behaviors of Δ_s , Δ_c and Δ_e as a function of $1/L$ for different U at $V = 1.0t$. For $V = 0.3t$, similar results can be drawn but the $V = 1.0t$ case is more accurate because most of the features can be seen when the chain length is short, while in the $V = 0.3t$ case, very long chains need to be used to obtain the same results. Figure 1 (a) presents the results for $U = 2.0t$ and clearly shows that the three gaps converge to the same finite value in the thermodynamic limit. The difference between these gaps shown in Fig. 1 (b) also displays this feature clearly. When the chain length is short, the exciton gap is larger than the spin gap, and level crossing happens at a finite chain length where the exciton gap drops lower thereafter. The exciton gap decreases continually and reaches a minimum when the chain length increases further; it then starts to increase and converge to the value of the spin and charge gaps. For $U = 3.0t$, in Fig. 1 (c) and (d), the spin gap and charge gap still converge to the same value in the thermodynamic limit, but the exciton gap goes to a different value lower than the other two gaps. In short chains, the exciton gap is still larger than the spin gap, but after they cross each other, the exciton gap decreases monotonically. One can also see that the second state in the singlet sector also crosses

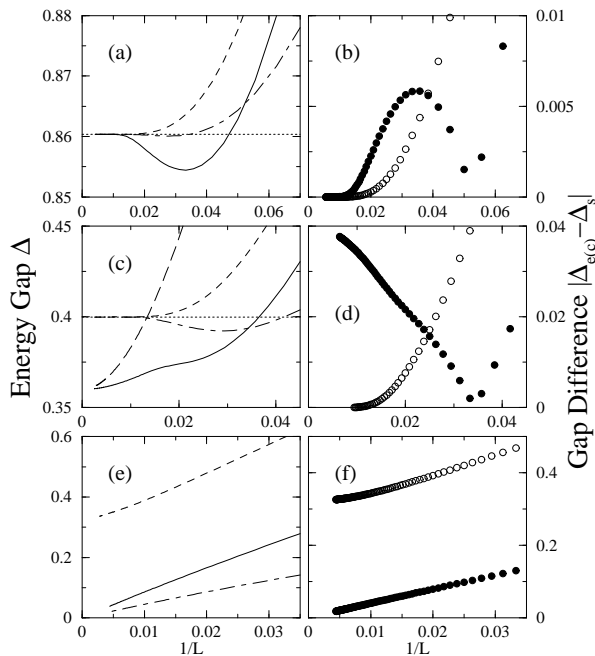


FIG. 1: Energy gaps vs $1/L$ for $V = 1.0t$ and (a) $U = 2.0t$, (c) $U = 3.0t$, (e) $U = 4.0t$. Solid lines are Δ_e , dot-dashed lines are Δ_s , and short-dashed lines are Δ_c . The long-dashed line in (c) represents the gap of the second state in the singlet sector $\Delta_c^{(2)}$. The dotted lines in (a) and (c) denote the thermodynamic limit of the corresponding gaps. Panels (b), (d), and (f) show the absolute values of the difference of the charge and exciton gap with the spin gap, where empty circles show $\Delta_c - \Delta_s$ and filled circles show $\Delta_e - \Delta_s$. 500 states are retained in the DMRG calculations.

the spin and charge gap and converges to the lowest state when $L \rightarrow \infty$. In our calculations, we also see that more states in the singlet sector cross the spin and charge gap with increasing chain length. This shows that the whole spectrum of the exciton sector decreases in value and the exciton gap is indeed different from the other two gaps. For the case of $U = 4.0t$, shown in Fig. 1 (e) and (f), no level crossing for different chain length is detected. All three gaps decrease monotonically when the chain length increases. The exciton gap and the spin gap approach zero at infinite chain length, indicating that there is no gap for the exciton and spin sectors. Meanwhile the charge gap approaches a finite value in the thermodynamic limit.

For all the cases we have studied, Δ_c decreases monotonically with increasing L . However, the size dependence of Δ_s is more complicated. In certain ranges of U/t and V/t close to the critical regimes, including the case shown in Fig. 1 (a) and (c), Δ_s and Δ_e vary non-monotonically and their minima are located at a finite $L = L_{\min}$ rather than at $L = \infty$. In a recent work²⁹, the authors studied the same model Hamiltonian (1) using the DMRG method but did not observe such non-monotonically behavior, and suggested that such a be-

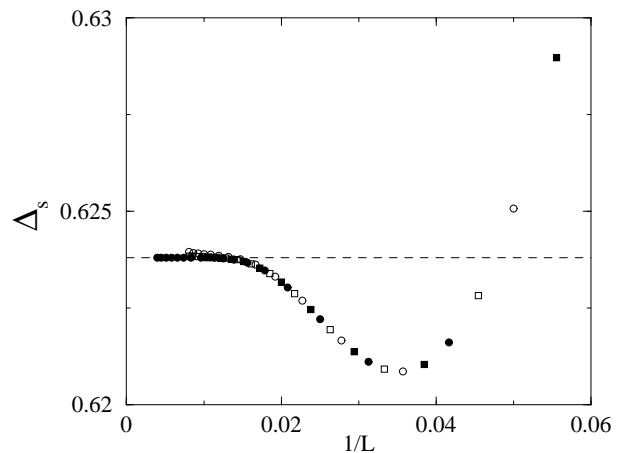


FIG. 2: The spin gap Δ_s vs $1/L$ for $V = 1.0t$ and $U = 2.50t$. The number of retained states are $m=300$ (empty circles), 400 (empty squares), 500 (filled circles), and 800 (filled squares).

havior may be due to the loss of accuracy in DMRG calculations when the chain length is increased or due to some intrinsic length scale for the spin degree of freedom. We have carefully examined this issue by carrying out extensive scaling analysis. We demonstrate that the non-monotonical behavior is not due to the lack of accuracy of the calculations, instead the behavior is a true feature of Hamiltonian (1) with the open boundary condition (OBC). Figure 2 shows the chain length dependence of the spin gap for $U = 2.5t$ and $V = 1.0t$ calculated by retaining different numbers of optimal states $m = 300, 400, 500$, and 800 . One can see that the minimum occurs at $L \sim 30$; at this length the accuracy of the DMRG calculations are still very high. More significantly, the results for different m fall onto the same curve (except for the cases of $L > 100$ and $m = 300$). It shows unambiguously the existence of the minimum of Δ_s in its dependence on the chain length. For the exciton gap Δ_e , the situation is the same. In fact the occurrence of a gap minimum at a finite L is not an uncommon feature for a system with incommensurate low-lying excitations. It suggests that the spin excitations of the model Hamiltonian (1) maybe incommensurate with a characteristic wave vector defined by $2\pi/L_{\min}$ (or $\pi - 2\pi/L_{\min}$) in some area of the phase space.

Comparing Fig. 1 (a) and (c), it is clear that there is a special point U_e , where the exciton gap begins to deviate from the spin gap (for $V = 1.0t, 2.0t < U_e < 3.0t$). In both cases, all three excitations are gapful. The system is in the same (BI) phase as the $U = 0$ case, where $\Delta_s = \Delta_c = \Delta_e = 2V$ in the thermodynamic limit. Here particle-hole excitations bound into excitons by the Coulomb interaction at $U > U_e$. Fig. 3 shows the difference $\Delta_s - \Delta_e$ for $V = 1.0t$ and $0.3t$. The fitting to DMRG results gives the critical value $U_e = 2.264t$ for $V = 1.0t$ and $U_e = 1.276t$ for $V = 0.3t$.

For finite L we find that Δ_c is always larger than Δ_s . In

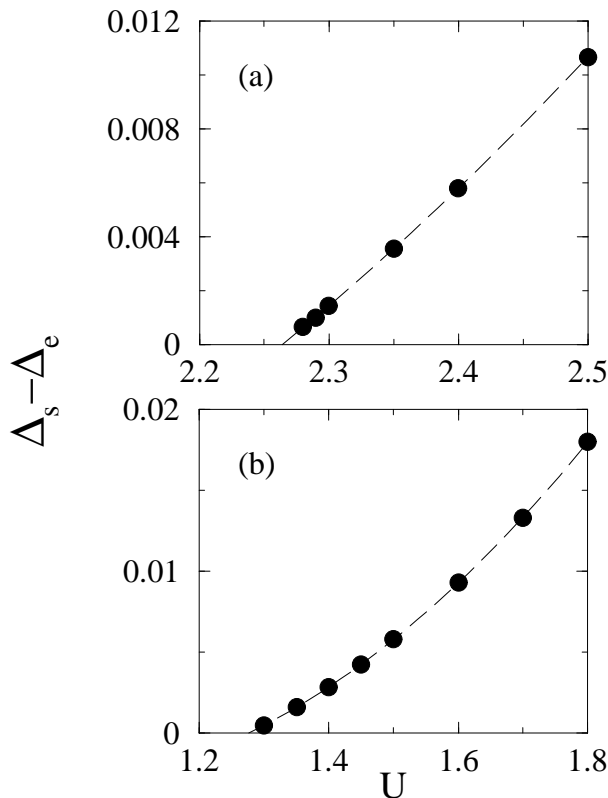


FIG. 3: The difference between the spin gap and the exciton gap near U_e . (a) $V=1.0t$, $U_e \sim 2.264t$. The dashed fitting line is $0.026(U/t - 0.771)(U/t - 2.264)$; (b) $V=0.3t$, $U_e \sim 1.276t$. The dashed fitting line is $0.0282(U/t - 0.584)(U/t - 1.276)$.

the MI phase, Δ_c is finite but Δ_s approaches zero in the thermodynamic limit. In the BI phase, Δ_s and Δ_c always approach the same value in the thermodynamic limit. This can be seen either from the asymptotic behaviors of Δ_s and Δ_c in the limit $L \rightarrow \infty$ [Fig. 1 (a) and (c)] or from the $1/L$ dependence of the difference $\Delta_c - \Delta_s$ (Fig. 1 (b) and (d)). For all the cases we have studied, we find that $\Delta_c - \Delta_s$ drops monotonically and approaches zero in the limit $1/L \rightarrow 0$ even when Δ_s changes non-monotonically. For a given V , this result holds from $U = 0$ up to a critical regime where both Δ_c and Δ_s become smaller than truncation errors. It suggests that Δ_c and Δ_s are equal in the thermodynamic limit in the entire BI phase.

When Δ_s changes non-monotonically with L , the extrapolation for the spin gap in the limit $1/L \rightarrow 0$ becomes subtle. If the data with $L < L_{\min}$ are used in the extrapolation, the extrapolated value of Δ_s will certainly be smaller than the true value. However, if the data with $L > L_{\min}$ is used but L is still not large enough to reach the regime where Δ_s begins to saturate, the extrapolated value of Δ_s will be larger than the true value (this seems to be the case in Ref. 27). For the data shown in Fig. 1(a) and (c), these two kinds of extrapolations result in $\Delta_c > \Delta_s$ and $\Delta_c < \Delta_s$, respectively. Both are incorrect.

To correctly extrapolate Δ_s in the limit $1/L \rightarrow 0$, data with L much larger than L_{\min} must be used.

For the $U = 4.0t$ case shown in Fig. 1 (e), Δ_c is finite but Δ_s becomes zero in the thermodynamic limit. This indicates that the system is in the same phase as that for $U \rightarrow \infty$, namely the MI phase. In the MI phase, the chain length dependence of the three gaps are monotonical; in addition, there is no crossing between Δ_s and Δ_e when the chain length varies. In the $L \rightarrow \infty$ limit the spin gap Δ_s is zero in the MI phase suggesting that there is a critical point that separates the MI phase from the BI phase. At this critical point U_s , the spin gap vanishes. Because the charge gap is equal to the spin gap in the BI phase, the charge gap will also vanish at the same point U_s . However, when U increases further, the charge gap increases with U while the spin gap remains zero. Considering that the exciton gap is lower than the spin gap in the BI phase at $U > U_e$, Δ_e may vanish before the spin gap and charge gap do. In that case, there should be another critical point U_c signaling the collapse of the exciton gap.

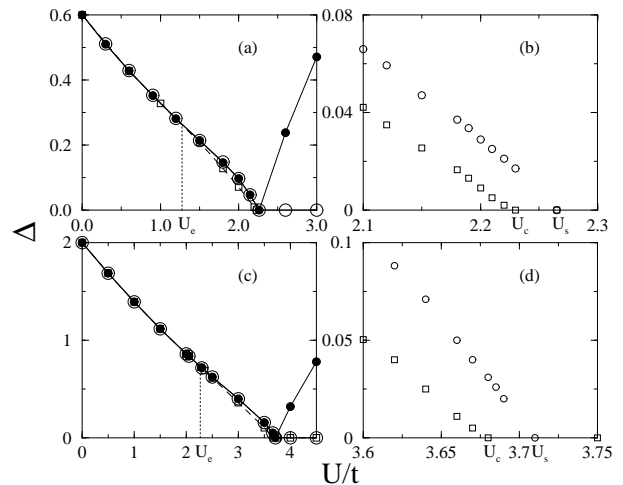


FIG. 4: The spin (empty circles), charge (solid circles) and exciton (empty squares) gaps as a function of U for $V = 0.3t$ (a) and $V = 1.0t$ (c). Panels (b) and (d) show the U dependence of the spin and exciton gaps in the vicinity of the critical region for (a) and (c) respectively. At U_e , the exciton gap deviates from the other two gaps and it collapses first at $U_c \sim 2.225t$ for $V = 0.3t$ and $\sim 3.675t$ for $V = 1.0t$. The charge and spin gaps collapse at $U_s \sim 2.265t$ for $V = 0.3t$ and $\sim 3.71t$ for $V = 1.0t$. For $0 < U < U_s$ the spin and charge gaps have the same value in the thermodynamic limit. When $U > U_s$, the spin and exciton gap are zero while the charge gap is finite.

In Fig. 4, we show the U dependence of the three gaps for $V = 0.3t$ [(a) and (b)] and $V = 1.0t$ [(c) and (d)]. For both cases, there are indeed two critical points U_c and U_s although they are very close. When $U < U_e$, $\Delta_e = \Delta_s = \Delta_c$, and the three gaps decrease almost linearly with increasing U . At U_e , the exciton gap splits off and drops below the other two gaps. At the critical point U_c ,

the exciton gap collapses while the spin and charge gaps still coincide and remain finite until the second critical point U_s where they both collapse. At $U > U_s$, the charge gap increases with increasing U while the spin gap and the exciton gap remain zero in the thermodynamic limit. Although the accuracy of our DMRG calculations do not allow a direct assessment of the behavior of the exciton gap for $U_c < U < U_s$, we believe that Δ_e is finite in this region (see more detailed discussion on this point in the following section). The extrapolation of the gap behavior leads to $U_c \sim 2.225t$ and $U_s \sim 2.265t$ for $V = 0.3t$, while $U_c \sim 3.675t$, $U_s \sim 3.71t$ for $V = 1.0t$.

It is clear that the U dependence of the three gaps is similar for $V = 0.3t$ and $V = 1.0t$. It is expected that the same picture is valid for all V . Furthermore, U_e , U_c , and U_s all approach the same point $U_\infty = 2V$ in the $V \rightarrow \infty$ limit.

IV. CRITICAL BEHAVIOR

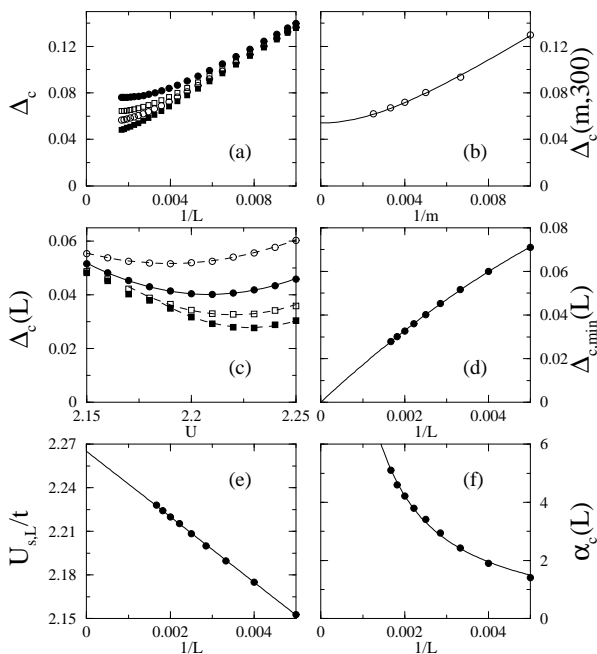


FIG. 5: The behavior of the charge gap in the vicinity of U_s for $V = 0.3t$. (a) The chain length dependence of the charge gap at $U = 2.2t$ for different numbers of optimal states retained: $m=200$ (filled circles), 250 (empty squares), 300 (empty circles) and 400 (filled squares); (b) The dependence of the charge gap on the number of the retained states at $L=300$ with $U = 2.2t$; (c) The charge gap for $m \rightarrow \infty$ with different chain lengths: $L = 300$ (empty circles), 400 (filled circles), 500 (empty squares) and 600 (filled circles) in the vicinity of the critical region; the fitting lines using eq. (8) are also shown; (d) The chain length dependence of $\Delta_{c,\min}(L)$; (e) The chain length dependence of $U_{s,L}/t$; (f) The chain length dependence of $\alpha_c(L)$.

From the gap behavior presented in the previous sec-

tion, it is clear that there are two critical points U_c and U_s for Hamiltonian (1) for a given V . It is important to study the detailed critical behavior near the critical points for the understanding of the nature of the BI-to-MI transition. In the following we study the critical behavior of the system by examining (i) the evolution of the gap behavior near the critical points and (ii) the behavior of the ground-state energy of the system.

A. Analysis of the gap behavior

The U dependence of the gaps shows that the charge instability occurs at the same point as that for the spin transition. To determine the critical points for the charge and spin excitations, we examine when Δ_c and Δ_s become zero in the limit $L \rightarrow \infty$. Since the numerical errors are larger than the magnitude of Δ_c or Δ_s in the vicinity of the critical points, it is difficult to determine accurately the critical behavior simply from the values of the energy gaps. To resolve this issue, we analyze the scaling behavior of $\Delta_c(L)$ around its minimum with respect to U . However, the DMRG results of $\Delta_c(L)$ depend the number of states m retained during the iterations. When the chain length is long enough, the difference due to retaining different number of states show clearly. In Fig. 5 (a), we show the chain length dependence of the charge gap at $U = 2.22t$ and $V = 0.3t$ by keeping different m . The difference is obvious. This problem can be solved by employing the extrapolation in the limit of $m \rightarrow \infty$. For given U and V , the charge gap at chain length L and by keeping m states is $\Delta_c(m, L)$. By extrapolating to the infinite m limit, more accurate result of the charge gap at chain length L can be obtained,

$$\Delta_c(\infty, L) = \lim_{m \rightarrow \infty} \Delta_c(m, L). \quad (7)$$

In Fig. 5 (b), we show the $1/m$ dependence and the extrapolation procedure of the $\Delta_c(m, L)$ for $L=300$ at $U = 2.22t$ and $V = 0.3t$. The extrapolated result $\Delta_c(\infty, L)$ is considered the exact charge gap $\Delta_c(L)$ at chain length L .

The extrapolated charge gap $\Delta_c(\infty, L)$ is a function of U and chain length L at a given V . By applying the same procedure shown in Fig. 5 (b), we obtain $\Delta_c(\infty, L)$ for different values of U near the critical point U_s for a serial of selected L . In Fig. 5 (c), we show the U dependence of $\Delta_c(L)$ ($\Delta_c(\infty, L)$) in the vicinity of the critical point U_s at chain length $L = 300, 400, 500$, and 600 , respectively, for $V=0.3t$. A gap minimum at finite chain length is clearly seen. Assuming $\Delta_{c,\min}(L)$ to be the minimum of $\Delta_c(L)$ located at $U_{s,L}$, then around this minimum we can expand $\Delta_c(L)$ to the leading order of the parameter $u = U - U_{s,L}$ as

$$\Delta_c(L) = \Delta_{c,\min}(L) + \alpha_c(L) u^2 + O(u^3). \quad (8)$$

Since $\Delta_c(L)$ is an analytic function of U , both $\Delta_{c,\min}(L)$ and $\alpha_c(L)$ should be finite. The critical behavior of

the charge excitations is determined by the properties of $\Delta_{c,\min}(L)$ and $\alpha_c(L)$ in the limit $L \rightarrow \infty$. If $\Delta_{c,\min}(L) \rightarrow 0$ in the limit $L \rightarrow \infty$, the charge excitation is critical at $U_s = U_{s,\infty}$, which would be consistent with the discussion in the previous section. However, if $\Delta_{c,\min}$ remains finite in the limit $L \rightarrow \infty$, then there is no critical point for charge excitations and the ground state is insulating in the entire parameter space.

Figure 5 (d) shows the calculated $\Delta_{c,\min}(L)$ as a function of $1/L$. The solid curve is a least-square fit of the data and given by $\Delta_{c,\min}(L) \approx 17.894/L - 729.785/L^2$. Within numerical errors, we find that $\Delta_{c,\min}(L)$ is indeed 0 in the limit $1/L \rightarrow 0$. Figure 5 (e) shows the L dependence of $U_{s,L}$. It changes almost linearly with $1/L$. Within numerical errors, we find that the data of $U_{s,L}$ are well fitted by $U_{s,L}/t \approx 2.265 - 22.532/L$. Thus the critical point is at $U_c/t = 2.265t$, in full agreement with the value obtained by fitting the gap directly in the previous section.

We now turn to the critical behavior of $\alpha_c(L)$. Figure 5 (f) shows the $1/L$ dependence of $\alpha_c(L)$ for the case $V = 0.3t$. The fitting curve (solid line) is given by $-0.323 + 0.0091L$. The divergence of $\alpha_c(L)$ suggests that the derivative of $\Delta_c(L)$ is singular at U_s and the leading term in Δ_c in the thermodynamic limit is linear rather than quadratical in u , i.e., $\Delta_c(U) \sim |U - U_s|$.

B. Analysis of the ground-state energy

The ground-state energy as the zero-temperature free energy can also provide evidence for the critical behavior. However, singularities in the ground-state energy are of higher order derivatives with respect to the model parameter for continuous phase transitions. As a result, evidence for critical behavior derived from the ground-state energy is not as strong as that from the gap behavior, this despite the higher accuracy of the ground-state energy than that for the gap in the DMRG calculations.

We have calculated the ground-state energy in the critical region by retaining $m=800$ states and up to chain length $L=1000$. For Hamiltonian (1), with open boundary conditions, the ground-state energy per site $e_0(L)$ satisfies

$$e_0(L) = \frac{E_0(L)}{L} = \epsilon_0 + \frac{e_b}{L} + \frac{c}{L^2} + O\left(\frac{1}{L^3}\right), \quad (9)$$

here $E_0(L)$ is the ground-state energy for a chain of length L , ϵ_0 the ground-state energy per site for $L \rightarrow \infty$, e_b is the boundary energy (surface energy) due to the free boundary condition, and $c = v\pi$ where v is the spin wave velocity. When $U > U_c$, the system is gapful and c should approach zero when the chain length is much larger than the correlation length ξ .

The $V = 0.3t$, $L > 200$ ground-state energy results are fitted directly by

$$e_0(L) = \epsilon_0 + e_b/L + c/L^2, \quad (10)$$

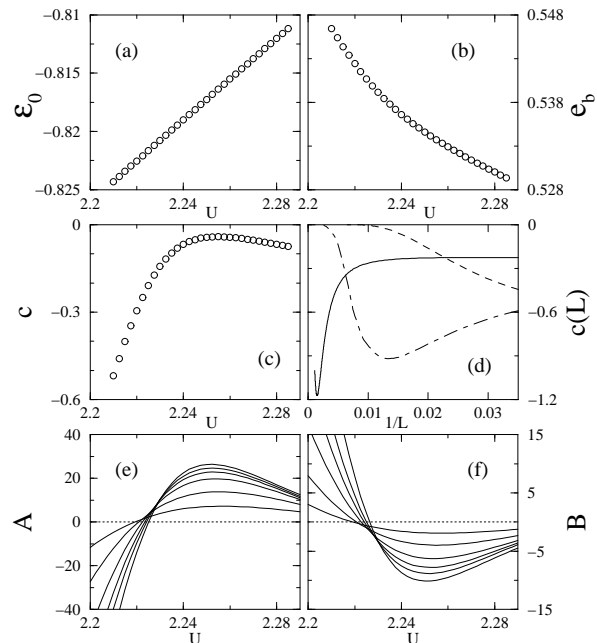


FIG. 6: (a), (b), (c): The U dependence of ϵ_0 , e_b and c obtained from fitting the $L > 200$ data of the ground-state energy; (d) The chain length dependence of $c(L)$ for $U = 1.5t$ (dashed line), $U = 2.0t$ (dot-dashed line), and $U = 2.2t$ (solid line); (e) $A = 10^6(\epsilon_0(L) - \epsilon_0(100))$ for $L=120, 150, 200, 250, 300,$ and 400 (from bottom to top on the $A > 0$ side); (f) $B = 10^3(e_b(L) - e_b(100))$ for the same chain lengths as in (e) (from top to bottom on the $B < 0$ side).

and the obtained results are shown in Fig. 6 (a), (b) and (c). ϵ_0 and e_b are analytic functions of U . For c , Fig. 6(c) shows that it is not only non-zero for $U < U_c$ but also has a fairly large value. This is due to the finite chain length effect. The value of c depends very sensitively on the chain length range used for fitting.

To analyze the chain length dependence of c , we fit the ground-state energy for $L - 20$, L , and $L + 20$ using Eq. (10) and vary L from 24 to 980. Each fitting gives the exact result of $\epsilon_0(L)$, $e_b(L)$ and $c(L)$. In Fig. 6(d), we show the L dependence of $c(L)$ for $U = 1.5t$, $U = 2.0t$ and $U = 2.2t$. It is clear that for $U = 1.5t$ and $2.0t$, $c(L)$ becomes zero when $L \rightarrow \infty$. The result of $U = 2.0t$ shows a minimum at $L \sim 90$, and the $c(L)$ begins to approach zero after the minimum. For $U = 2.2t$, a minimum is also clearly seen. A comparison of these results leads to the conclusion that for $L \rightarrow \infty$, $c(L)$ will approach zero. The largest chain length used in the calculation is not long enough to obtain correct $c(L)$ values. However, the obtained $\epsilon_0(L)$ and $e_b(L)$ may display the critical behavior of U_c and U_s . In Fig. 6 (e) and (f), we show the results of $\epsilon_0(L) - \epsilon_0(L_0)$ and $e_b(L) - e_b(L_0)$ for $L_0 = 100$. These results show the existence of the critical point U_c . L_0 can be viewed as a characteristic length of the critical region.

From the U dependence of ϵ_0 , it is possible to examine

the type of transition at the critical points. A problem is that the fitting results shown in Fig. 6(a) include extra errors induced by the fitting method. To avoid this, we analyze the U dependence of the ground-state energy using a different approach.

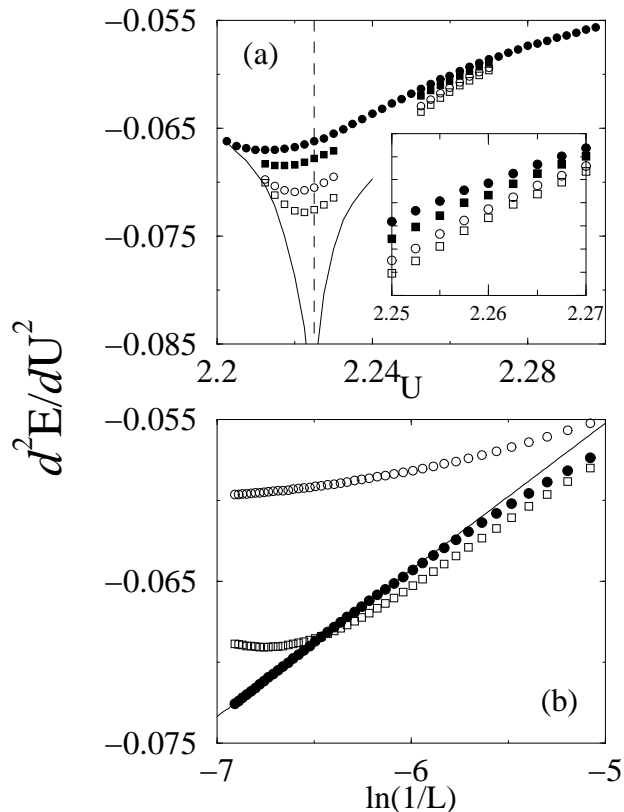


FIG. 7: (a) $d^2 e_0 / dU^2$ versus U for $L = 500$ (filled circles), 600 (filled squares), 800 (empty circles), 1000 (empty squares). The solid line is an extrapolation of the data to the limit $L \rightarrow \infty$. Inset: Enlarged figure in the vicinity of the critical point U_s . (b) The dependence of the $d^2 e_0 / dU^2$ with $\ln(1/L)$ at $U = 2.21t$ (empty squares), $2.225t$ (filled circles), $2.27t$ (empty circles). The solid fitting $-0.00997 + 0.009 \ln(1/L)$ is the least square fitting for the $U = 2.225t$ case.

At a finite chain length L , the ground-state energy per site $e_0(L)$ is also a function of U . Here $e_0(L)$ contains only the errors from the DMRG truncation. We can examine the derivatives of $e_0(L)$ with respect to U and analyze their chain length dependence. In Fig. 7(a), we show the second derivative of $e_0(L)$ with U for $L=500$, 600, 800, and 1000. At each chain length, there is a minimum near U_c in the U dependence of the second derivative. When the chain length increases, the position of the minimum moves towards larger U and approaches U_c which is the critical point in the thermodynamic limit; meanwhile, the shape of the minimum becomes sharper. Fig. 7(b) shows the chain length dependence of the second derivative. It is clear that for $U = 2.225t \sim U_c$, the second derivative diverges logarithmically with the chain length, but for other values of U the second deriva-

tive does not diverge. These observations suggest that the phase transition at U_c is of the second order. No singularity is found in the first derivative or the second derivative near the critical point U_s . This means that the transition at U_s is higher than second order. These results are consistent with those reported by Fabrizio *et al.*¹⁸.

V. TMRG STUDY OF SPIN SUSCEPTIBILITY AND SPECIFIC HEAT

To gain more insight into the physics of the BI-to-MI transition, we have studied the thermodynamic properties of the model using the TMRG method^{23,24,25} which is implemented in the thermodynamic limit and can evaluate very accurately the thermodynamic quantities at low temperature for quasi-1D systems. In our calculations, we kept 250 optimal states. The calculated specific heat C_v , charge susceptibility χ_c , and spin susceptibility χ_s for $U/t = 1.0, 2.25, 5.0$ and $V/t = 0.3$ as a function of temperature are shown in Fig. 8.

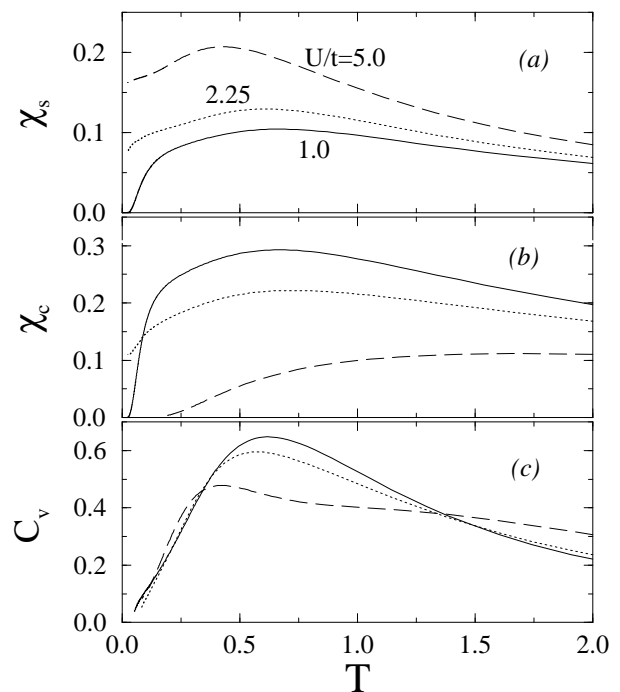


FIG. 8: Temperature dependences of (a) the spin susceptibility χ_s , (b) the charge susceptibility χ_c , and (c) the specific heat C_v . (t is set to 1).

We find that χ_c decreases exponentially at low temperatures in both the BI and MI phases, while χ_s shows activated behavior only in the BI phase. In the MI phase, there are two broad peaks in C_v , probably due to the charge-spin separation. Near the critical point, $U=2.25t$, since both the charge and spin energy gaps are very small, the exponential decays in both χ_c and χ_s show up only

at very low temperatures. These results support the conclusions of the DMRG calculations presented in previous sections.

VI. PHASE DIAGRAM

The overall U dependence of the charge, spin and excitation gaps shown in Fig. 4 give a lot of information on the phase diagram of Hamiltonian (1). The charge and spin gaps coincide in the BI phase. Above U_s , Δ_c increases with U but Δ_s remains zero. The exciton gap Δ_e collapses at $U_c < U_s$, and when $U > U_s$, the exciton gap should also be zero. However, from Fig. 4 it is unclear whether the exciton excitations are gapful or gapless in the regime between the two critical points, $U_c < U < U_s$. Even if the exciton excitations are gapful in this regime, the gap would be too small to detect numerically.

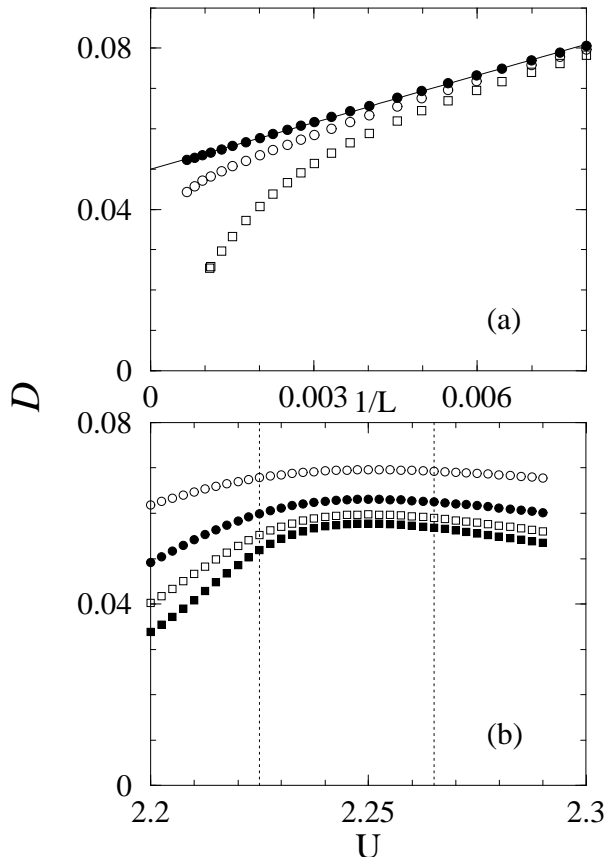


FIG. 9: (a) Chain length dependence of the dimerization order parameter \mathcal{D} for $U = 2.21t$ (empty squares), $U = 2.25t$ (filled circles) and $U = 2.29t$ (empty circles). The straight fitting line is $0.0499 + 3.886/L$. (b) $\mathcal{D}(L)$ in the critical regime for $L=200$ (empty circles), 300 (filled circles), 400 (empty squares), and 500 (filled squares). The dotted lines indicate the two critical points.

When the exciton gap collapses, the excitons can condense into the ground state³⁰. In this case, the system is

expected to be dimerized¹⁸. Here we evaluate the dimerization order parameter

$$\mathcal{D} = \frac{1}{L} \sum_{i\sigma} (-1)^i (c_{i\sigma}^\dagger c_{i+1\sigma} + h.c.). \quad (11)$$

Figure 9(a) shows the chain length dependence of the dimerization operator for different U . It is clear that for $U = 2.21t$, when $L \rightarrow \infty$, \mathcal{D} approaches zero. At $U = 2.29t$, \mathcal{D} just starts to fall at the largest chain length we studied; it is expected that it will approach zero as the chain length is long enough. For $U = 2.25t$, which is between the two critical points, it seems that \mathcal{D} will diverge to a nonzero constant. For a large range of chain lengths, the results can be well fitted by a straight line shown in Fig. 9 (a). The dependence of the finite chain dimerization $\mathcal{D}(L)$ on U is shown in Fig. 9(b) for $L=200$, 300, 400, and 500. These results indicate that in the thermodynamic limit, the ground states are dimerized when $U_c < U < U_s$.

The dimerization of the ground state for $U_c < U < U_s$ suggests that the exciton excitations are gapful in this region. So the physical picture on the exciton excitation is emerging: the exciton gap formed in the BI phase collapses at the critical point U_c ; with further increasing U , the (small) exciton gap will first increase, reach a maximum and then decrease and collapse again at U_s ; at $U > U_s$, the exciton excitations remain critical.

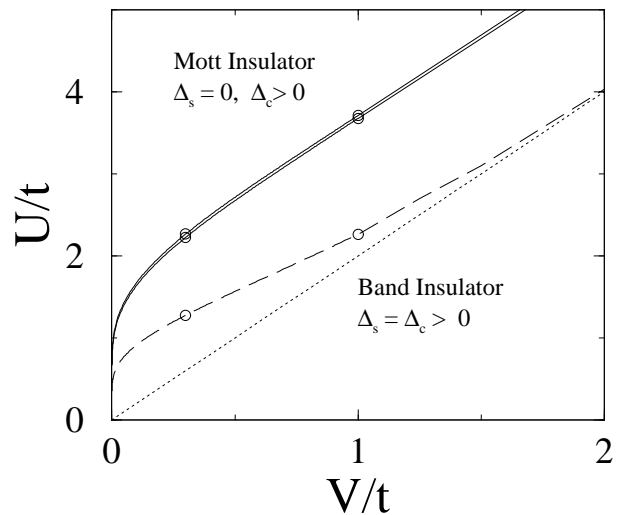


FIG. 10: The ground-state phase diagram for Hamiltonian (1). The empty circles denote the DMRG results. The curves of U_s and U_c are shown with solid lines that are very close to each other. The curve of U_e is shown by the dashed line which does not indicate a phase transition line, but rather denotes a series of special points. The dotted line is $U = 2V$ which is the limit for $V \rightarrow \infty$.

When $U \ll V$, first order perturbation leads to

$$\Delta_s(U) = \Delta_c(U) \approx V - cU, \quad (12)$$

where $c = V \int_0^\pi dk (\sqrt{2\pi\varepsilon_k})^{-1}$ is a constant determined by the single-particle energy dispersion $\varepsilon_k = \sqrt{V^2 + 4t^2 \cos^2 k}$. Since $\Delta_c(U)$ drops almost linearly with U/t in the BI phase, we can estimate the value of U_s from Eq. (12) as $U_s \approx V/c$. In the limit $V \rightarrow 0$, we have

$$V/t \approx c_1 e^{-c_2 t/U_s}, \quad \text{or} \quad U_s/t \approx -\frac{c_2}{\log(V/c_1 t)}, \quad (13)$$

where c_1 and c_2 are two constants of order one. Figure 10 shows the ground-state phase diagram for Hamiltonian (1). The curve for U_s and $V < 1.0t$ is obtained from Eq. (13). The parameters c_1 and c_2 are fixed by the two U_s values for $V = 0.3t$ and $V = 1.0t$. When $V \rightarrow 0$, U_s goes to zero but the ratio U_s/V diverges. In the limit $U/t \rightarrow \infty$, U_s is very close to $2V$. The difference between U_s and $2V$ is of order t : $U_s - 2V \sim t$.

VII. SUMMARY

We have carried out systematic studies using the DMRG and TMRG methods to examine the critical behavior of a one-dimensional Hubbard model with an alternating site potential in the transition from band insulator to Mott insulator. Based on extensive numerical calculations and analytic analysis, we have clarified sev-

eral important issues raised in recent works and have established the ground-state phase diagram. We have identified two critical points, U_c and U_s , that separate the BI and MI phases. When $U > U_s$, the system is in the MI phase where the charge excitations are massive but the spin excitations are critical. When $U < U_c$, the system behaves like a classic band insulator: the charge and spin excitation gaps coincide and a charge-neutral spin-singlet exciton band forms below the band gap when U exceeds a special point U_e . Between the two critical points, excitons condense and the ground state is dimerized. These results are consistent with the conclusions of a recent field theoretical study of the same model. The present work provides a detailed account for the critical behavior in the BI-to-MI transition in one dimension for correlated electron systems and establishes a good understanding for its ground-state phase diagram.

Acknowledgments

We thank Y. L. Liu, R. Noack, and M. Fabrizio for helpful discussions and M. Tsuchiizu for bringing to our attention Refs. 9 and 11. This work was supported in part by the Department of Energy at the University of Nevada, Las Vegas, the NSF of China and the Special Funds for Major State Basic research Projects of China.

-
- ¹ J. Solyom, *Adv. Phys.* **28**, 201 (1979).
² F. D. M. Haldane, *J. Phys. C* **14**, 2585 (1981).
³ T. Egami, S. Ishihara, and M. Tachiki, *Science* **261**, 1307 (1993).
⁴ N. Nagaosa and J. Takimoto *J. Phys. Soc. Jpn.* **55**, 2735 (1986); **55**, 2745 (1986); N. Nagaosa, *ibid.* **55**, 2754 (1986); **55**, 3488 (1986).
⁵ S. Ishihara, T. Egami, and M. Tachiki, *Phys. Rev. B* **49**, 8944 (1994); S. Ishihara, M. Tachiki, and T. Egami, *ibid.* **49**, 16123 (1994).
⁶ G. Ortiz and R. Martin, *Phys. Rev. B* **49**, 14202 (1994); G. Ortiz, P. Ordejón, R. Martin, and G. Chiappe, *ibid.* **54**, 13515 (1996).
⁷ K. Schönhammer, O. Gunnarson and R.M. Noack, *Phys. Rev. B* **52**, 2504 (1995).
⁸ R. Resta, and S. Sorella, *Phys. Rev. Lett.* **74**, 4738 (1995); *ibid.* **82**, 370 (1999).
⁹ M. Tsuchiizu and Y. Suzumura, *J. Phys. Soc. Jpn.* **68**, 3966 (1999).
¹⁰ M. Nakamura, *Phys. Rev. B* **61**, 16377 (2000).
¹¹ M. Tsuchiizu and A. Furusaki, *Phys. Rev. Lett.* **88**, 56402 (2002); M. Tsuchiizu and Y. Suzumura, *J. Phys. Soc. Jpn.* **68**, 3966 (1999).
¹² T. Wilkens and R. M. Martin, *Phys. Rev. B* **63**, 235108 (2001).
¹³ Y. Anusooya-Pati and Z. G. Soos, *Phys. Rev. B* **63**, 205118 (2001).
¹⁴ K. Yonemitsu, *Phys. Rev. B* **65**, 85105 (2002).
¹⁵ S. Caprara, M. Avignon, O. Navarro, *Phys. Rev. B* **61**, 15667 (2000).
¹⁶ M. E. Torio, A. A. Aligia, and H. A. Ceccatto, *Phys. Rev. B* **64**, 121105 (2001).
¹⁷ N. Gidopoulos, S. Sorella and E. Tosatti, *Eur. Phys. J. B* **14**, 217 (2000).
¹⁸ M. Fabrizio, A. O. Gogolin, and A. A. Nersesyan, *Phys. Rev. Lett.* **83**, 2014 (1999).
¹⁹ M. Avignon, C. A. Balseiro, C. R. Proetto, and Alascio, *Phys. Rev. B* **33**, 205 (1986).
²⁰ R. Resta, *Rev. Mod. Phys.* **66**, 899 (1994).
²¹ J. B. Torrance, J. E. Vazques, J. J. Mayerle, and V. Y. Lee, *Phys. Rev. Lett.* **46**, 253 (1981); Y. Anusooya-Pati and Z. G. Soos, *Phys. Rev. B* **63**, 205118 (2001); K. Yonemitsu, *Phys. Rev. B* **65**, 085105 (2002).
²² S. R. White, *Phys. Rev. Lett.* **69**, 2863 (1992); *Phys. Rev. B* **48**, 10345 (1993).
²³ R. J. Bursill, T. Xiang, and G. A. Gehring, *J. Phys. Cond. Mat.* **8**, L583 (1996).
²⁴ X. Wang and T. Xiang, *Phys. Rev. B* **56**, 5061 (1997).
²⁵ N. Shibata, *J. Phys. Soc. Jpn.* **66**, 2221 (1997).
²⁶ F. H. L. Essler, V. E. Korepin, and K. Schoutens, *Nucl. Phys. B* **384**, 431 (1992).
²⁷ Y. Takada and M. Kido, *J. Phys. Soc. Jpn.* **70**, 21 (2001).
²⁸ T. Xiang and N. d'Ambrumenil, *Phys. Rev. B* **46**, 11179 (1992).
²⁹ Ph. Brune, G. I. Japaridze, A. P. Kampf, and M. Sekania, *cond-mat/0106007*.
³⁰ I. Affleck, *Phys. Rev. B* **43**, 3215 (1991).